Warping of Saturn's magnetospheric and magnetotail current sheets

C. S. Arridge,[1,2,3] K. K. Khurana,[4] C. T. Russell,[4] D. J. Southwood,[4,5] N. Achilleos,[3,6] M. K. Dougherty,[3] A. J. Coates,[1,2] and H. K. Leinweber[4]

Received 11 December 2007; revised 3 April 2008; accepted 30 May 2008; published 15 August 2008.

[1] The magnetotails of Jupiter and Earth are known to be hinged so that their orientation is controlled by the magnetic field of the planet at small distances and asymptotically approach the direction of the flow of the solar wind at large distances. In this paper we present Cassini observations showing that Saturn's magnetosphere is also similarly hinged. Furthermore, we find that Saturn's magnetosphere is not only hinged in the tail but also on the dayside, in contrast to the Jovian and terrestrial magnetospheres. Over the midnight, dawn, and noon local time sectors we find that the current sheet is displaced above Saturn's rotational equator, and thus the current sheet adopts the shape of a bowl or basin. We present a model to describe the warped current sheet geometry and show that in order to properly describe the magnetic field in the magnetosphere, this hinging must be incorporated. We discuss the impact on plasma observations made in Saturn's equatorial plane, the influence on Titan's magnetospheric interaction, and the effect of periodicities on the mean current sheet structure.

Citation: Arridge, C. S., K. K. Khurana, C. T. Russell, D. J. Southwood, N. Achilleos, M. K. Dougherty, A. J. Coates, and H. K. Leinweber (2008), Warping of Saturn's magnetospheric and magnetotail current sheets, *J. Geophys. Res.*, *113*, A08217, doi:10.1029/2007JA012963.

1. Introduction

[2] The most obvious magnetospheric asymmetry is the day-night asymmetry produced by the solar wind, compressing the dayside and stretching the nightside out into the magnetotail. When the solar wind flow and the dipole moment are not perpendicular, solar wind forcing also produces north-south asymmetries in the magnetosphere. At Earth and Jupiter, this is observed as a deflection of the magnetotail, which becomes asymptotically parallel to the solar wind flow at sufficiently large distances in the anti-sunward direction [*Khurana*, 1992; *Tsyganenko and Fairfield*, 2004].

[3] Mechanical stresses exerted on the magnetospheric plasma can also deform the structure of the field. In the Jovian magnetosphere, centrifugal stresses beyond $20R_J$ are sufficient to bend the magnetodisc [e.g., *Smith et al.*, 1974; *Hill et al.*, 1974] such that it becomes parallel to the rotational equator; however, the solar wind forcing on the current sheet largely overwhelms this process in determining the overall configuration [*Khurana*, 1992].

[4] The existence of nonzero planetary obliquities and tilts between the magnetic dipole and spin axes (dipole tilts) produces seasonal and diurnal periodicities in the net tilt angle between the dipole equator and the solar wind (herein referred to as the magnetospheric tilt). Consequently, these periodicities produce corresponding variations in the external and internal forcing mechanisms. The diurnal periodicities are produced by the rotation of the planet, causing the magnetic dipole axis to sweep once around the spin axis per rotation. The seasonal periodicities are driven by the obliquity of the planet, causing the tilt between the planet's spin axis and the solar wind to vary approximately sinusoidally with time between solstices. Hence the instantaneous magnetospheric tilt is a function of both planetary rotational and orbital phase. Since each of the magnetized planets has a differing obliquity and dipole tilt there is a spectrum of diurnal and seasonal periodicities amongst the planetary magnetospheres in the solar system. Figure 1 illustrates the range of obliquities and dipole tilts in the solar system (including Ganymede's magnetosphere, embedded in the Jovian magnetosphere, where its obliquity is equal to its orbital inclination due to its zero axial tilt).

[5] The Earth has comparatively equal oscillations, produced by a dipole tilt of $\approx 10^\circ$ and an obliquity of $\approx 23^\circ$. Detailed models for the orientation and motion of the Earth's magnetotail have been constructed [e.g., *Tsyganenko*, 1998; *Tsyganenko and Fairfield*, 2004] which also account for a wide range of solar wind conditions since reconnection with the interplanetary magnetic field also

[1] Mullard Space Science Laboratory, University College London, Dorking, UK.
[2] Centre for Planetary Sciences, University College London, London, UK.
[3] Space and Atmospheric Physics Group, Blackett Laboratory, Imperial College London, London, UK.
[4] Institute of Geophysics and Planetary Physics, University of California, Los Angeles, California, USA.
[5] European Space Agency, Paris, France.
[6] Atmospheric Physics Laboratory, University College London, London, UK.

0148-0227/08/2007JA012963

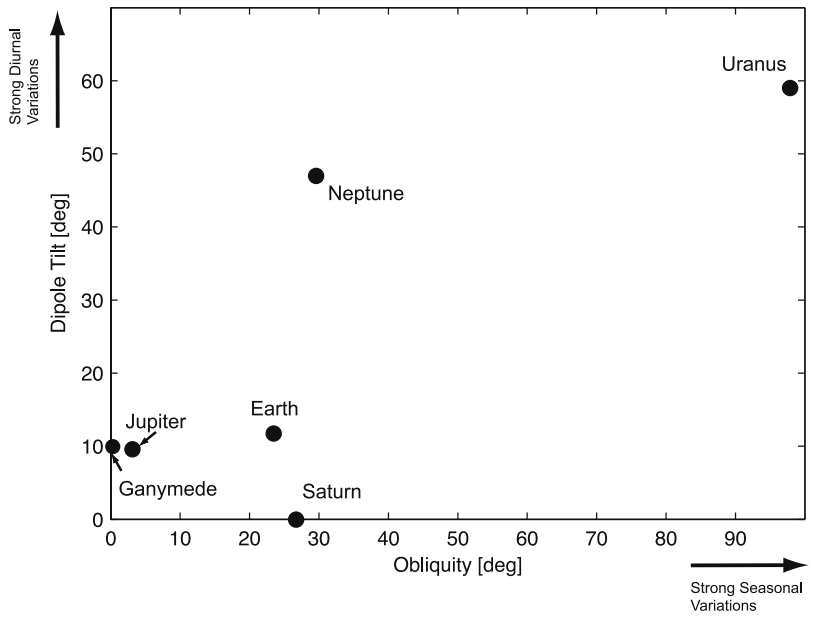

Figure 1. The parameter space formed by the tilt of a planetary dipole to the rotation axis and the obliquity of the planet. This figure illustrates this parameter space for the magnetized bodies of the solar system and shows that Jupiter should experience small seasonal and large diurnal variations, but Saturn should experience the exact opposite. Earth experiences both large diurnal and seasonal variability. Values for the planets are taken from *Bagenal* [1992] and values for Ganymede's dipole tilt and obliquity are taken from *Kivelson et al.* [1998] and the Astronomical Almanac Online 2008 (produced by the U.S. Naval Observatory and H.M. Nautical Almanac Office), respectively.

produces stresses inside the magnetospheric cavity which tend to bend and twist the magnetotail.

[6] Both Uranus and Neptune present extreme examples in the solar system. Neptune presents the most rapidly varying case in the solar system where its 29.6° obliquity and 47° dipole tilt conspire to point the dipole sunward and then antisunward over the course of one planetary rotation. When the dipole is approximately parallel to the solar wind the magnetotail forms a cone in the downtail direction with its apex at the planet [*Bagenal*, 1992]. A more classical magnetotail is formed at intermediate points in Neptune's sidereal rotation. Jupiter's relatively small obliquity produces very small seasonal oscillations compared to the large diurnal variations caused by the planet's ≈10° dipole tilt. Significant internal plasma stresses and time-dependent effects cause the magnetic equator to adopt a complex three-dimensional shape. Here the magnetic equator is defined as the surface on which the field ($\mathbf{B}_\rho$, [*Vasyliunas*, 1983]) associated with the current sheet reverses. Under moderately distorted conditions this is equivalent to a reversal in B_r and B_ϕ in cylindrical coordinates where the (r, ϕ) plane lies in the magnetic dipole equator.

[7] Saturn presents the opposite case to Jupiter in the dipole tilt-obliquity parameter space because of its small dipole tilt and large 26.7° obliquity. Figure 2 shows Saturn's magnetospheric tilt angle between 1975 and 2010 covering the period from before the Pioneer 11 flyby to after the end of Cassini's nominal mission. Close to equinox, Saturn's magnetosphere should be largely azimuthally symmetric apart from the day-night local time asymmetry produced by the solar wind, and possible (as yet uncharacterized) dawn-dusk asymmetries. Saturn was close to equinox during the Pioneer and Voyager flybys and the largest magnetospheric tilt during this epoch occurred during the Voyager 2 flyby when the tilt was 8.1° (positive sunward). Hence any seasonal effects should have been relatively weak in the in situ data and seasonal effects have not attracted significant attention in the literature.

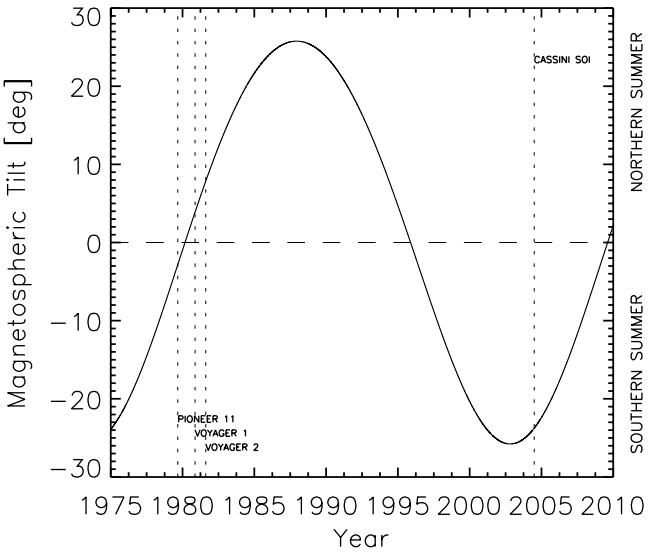

Figure 2. Magnetospheric tilt angle for Saturn between 1975 and 2010. The very small tilt between the dipole and spin axes at Saturn produces very little diurnal oscillation leaving only the 30 year seasonal periodicities.

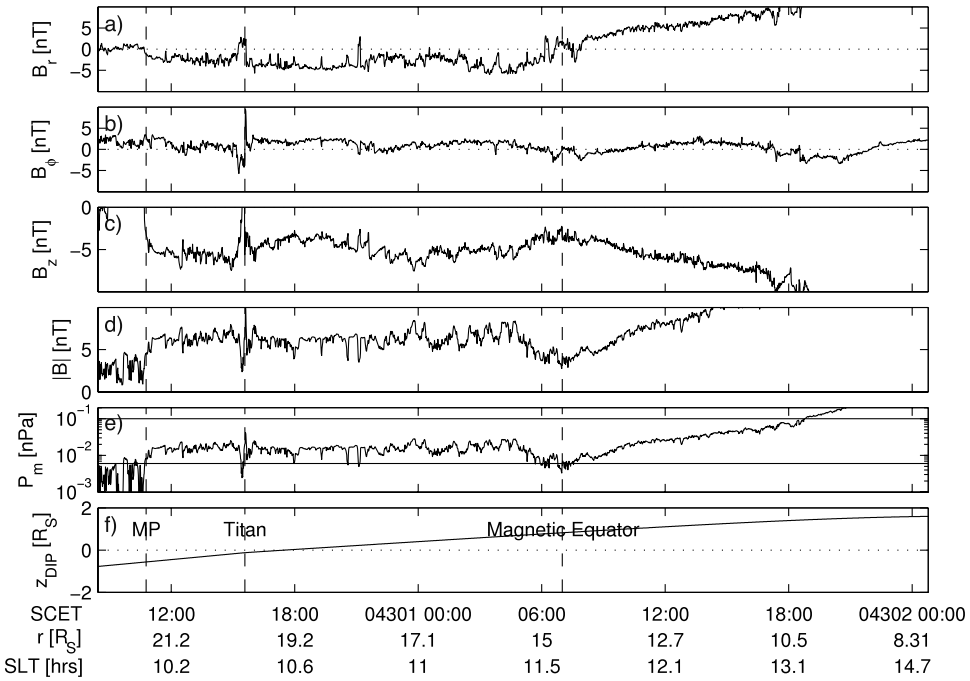

Figure 3. Cassini magnetometer data from Cassini's Rev A (26–28 October 2004, day 300–302). (a–c) The magnetic field in cylindrical polar coordinates, (d) the magnetic field strength, (e) the magnetic pressure (with the range of solar wind dynamic pressures indicated by the horizontal lines), and (f) the vertical distance from the dipole magnetic equator. The X axis values show the time in YYDOY and HH:MM, the radial distance of Cassini from Saturn, and the local time of Cassini.

[8] Cassini's Saturn Orbit Insertion (SOI) occurred shortly after (northern winter) solstice. Hence, if any seasonal effects are present in Saturn's magnetosphere they should be most strongly expressed and readily observable during the early part of the Cassini tour. In this paper we present observations showing that Saturn's magnetosphere is considerably warped at all local times. In each local time quadrant we find that Saturn's magnetospheric current sheet is displaced above the rotational equator thus forming a bowl or basin-type shape, similar to a paraboloid of revolution. The observed warping on the dayside is entirely unexpected and quite different to the warping of the Jovian magnetosphere.

[9] The paper is organized as follows: in section 2 we present and discuss magnetometer data showing the warping of the magnetosphere and in section 3 we present a model for the bowl-shaped current sheet. This model is applied to a simple axisymmetric current sheet model in section 4 and we show that the warping of the model ring current results in greatly improved fits to the magnetometer data. We will discuss our results, future work, and the wider implications of our findings in section 5.

2. Observations and Interpretation

2.1. Observations

[10] Figure 3 shows Cassini magnetometer [*Dougherty et al.*, 2004] data from the second orbit (Rev A) of Cassini and covers the period from the first inbound magnetopause crossing to a radial distance of $8R_S$ shortly before periapsis (26 October to 28 October 2004). The location of Cassini will be shown with respect to the dipole magnetic equator rather than the rotational equator of Saturn. The dipole equator is the symmetry plane for the planetary magnetic field and at Saturn is offset by $g_2^0/2g_1^0 = 0.04R_S$ from the rotational equator [*Dougherty et al.*, 2005]. The distance of Cassini from the dipole magnetic equator is plotted in Figure 3f and shows that Cassini crosses the equator shortly after an encounter with Titan at around 1530 UT on 26 October. However, this equator crossing is not associated with a reversal in sign of B_r which (for moderately distorted current sheet geometry) should accompany a change from one magnetic hemisphere to another. The reversal in B_r is observed 12 h later at a radial distance of $\sim 14.5R_S$. The radial field undergoes numerous oscillations in sign over the broad period of the current sheet crossing, indicative of vertical flapping motions with a period of 10 to 20 min.

[11] Throughout the interval up to and beyond the actual crossing of the magnetic equator the magnetic pressure inside the magnetosphere (Figure 3e) lies within the range of solar wind dynamic pressures observed at the magnetopause, corresponding to an observed range of standoff distances of $16R_S$ to $30R_S$ [*Arridge et al.*, 2006].

[12] Figure 4 shows magnetometer data from the outbound pass of Rev 3 from $8R_S$ out to the first magnetopause crossing near $40R_S$, covering the interval 17–25 February 2005. The field adopts a highly stretched configuration beyond $14R_S$ up to the magnetopause which is due to the field produced by Saturn's magnetodisc current sheet [*Arridge et al.*, 2008]. In Figure 4 the sign of B_r is consistently negative indicating Cassini is on field lines that are pointing toward the planet, i.e., in the southern magnetic hemisphere. There is a clear antiphase relationship between B_r and B_ϕ. Cassini is northward of the dipole

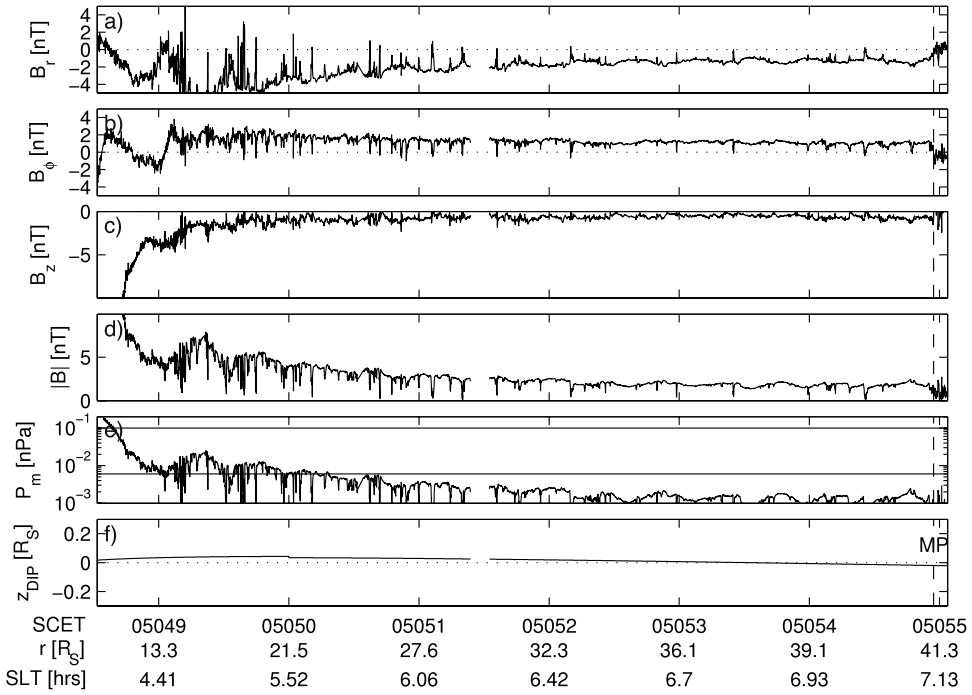

Figure 4. Magnetometer data from Cassini's Rev 3 (17–25 February 2005, day 048–056). (a–f) The plot is in the same format as Figure 3 but note the different scales on the ordinate axes in Figure 4f.

magnetic equator over the entire interval, except for about 22 h prior to the first outbound magnetopause crossing. Note that the magnetic pressure lies in the range of solar wind dynamic pressures as it was in Figure 3.

[13] Figure 5 shows data from Rev 26 in the magnetotail over a radial range of approximately $8R_S$ from 18 to 20 July 2006. Clear periodic crossings of Saturn's magnetotail current sheet are observed approximately every 11 h. Over the interval Cassini is approximately $0.25R_S$ ($0.2R_S$) northward of the rotational (magnetic dipole) equator. From the double-peaked form of the current sheet crossings Cassini is southward of the mean location of the current sheet [e.g., *Waldrop et al.*, 2005].

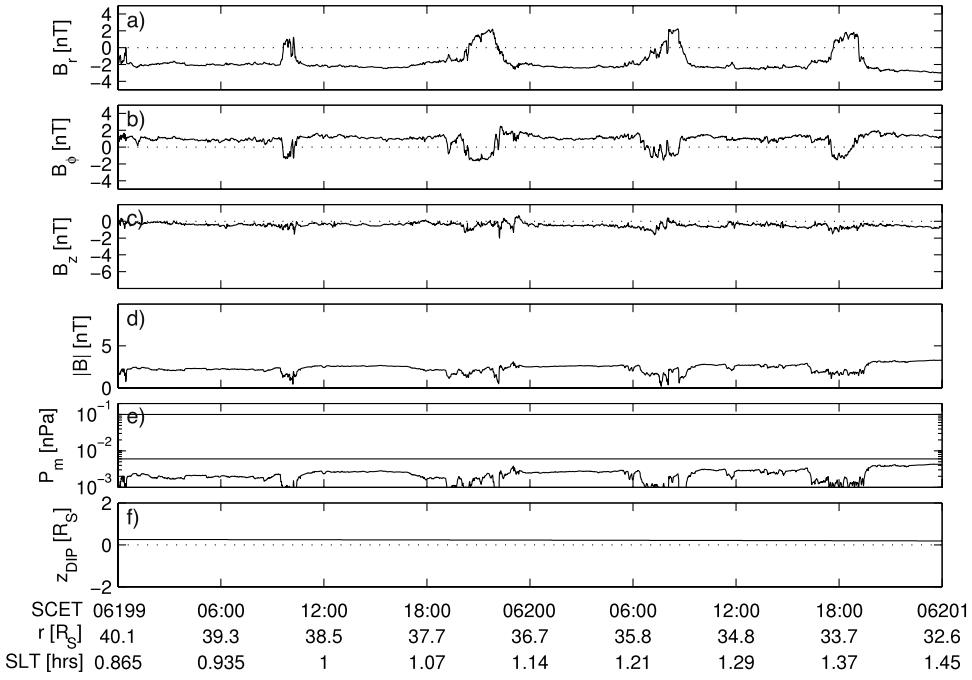

Figure 5. Magnetometer data from Cassini's Rev 26 (18–20 July 2006, day 199–201). The plot is in the same format as Figures 3 and 4.

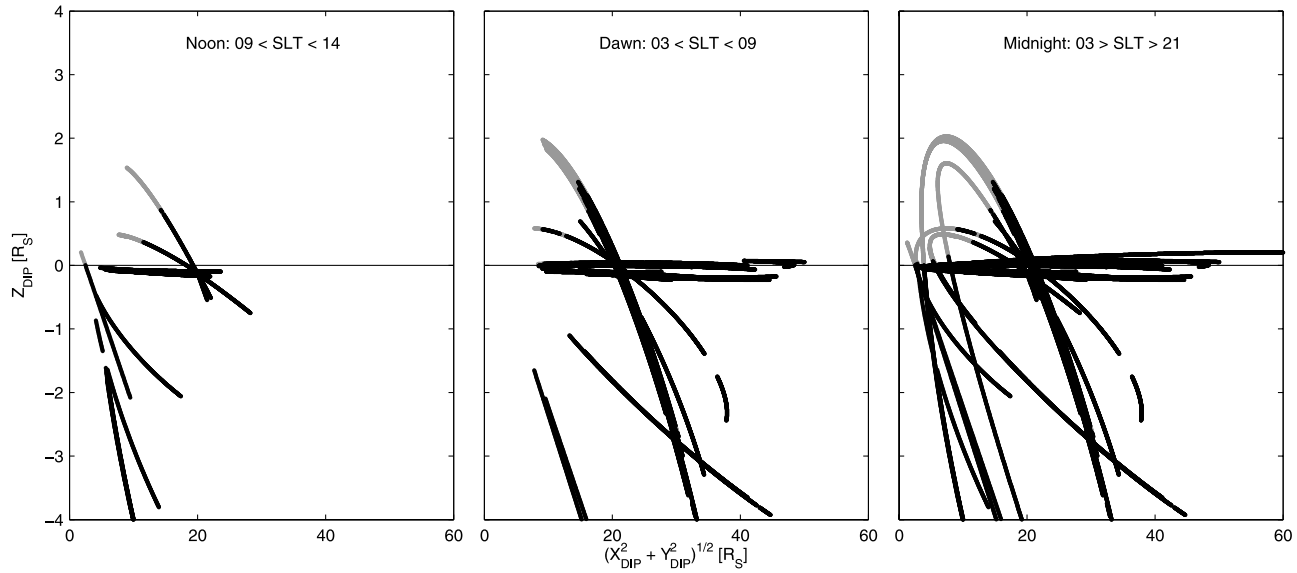

Figure 6. Cassini trajectories inside the magnetosphere between 30 June 2004 and 11 April 2006 divided into three local time sectors. Distance above and below the magnetic dipole equator is on the ordinate axis and distance from the spin axis as abscissa. Black segments of the trajectory indicate negative radial fields and gray indicates zero or positive. For a current sheet located in the dipole magnetic equator, we would expect gray above Z_{DIP} and black below. This is not what is observed.

[14] Hence beyond a certain radial distance in the noon, dawn, and midnight meridians, Cassini is located southward of the magnetospheric current sheet and magnetic equator even when in, or northward of, the dipole magnetic equator. The magnetic equator is the actual surface where B_r and B_ϕ reverse and is not the planar surface like the dipole magnetic equator. The analysis reported thus far has assumed that the symmetry plane for the current sheet should be the dipole magnetic equator. However, centrifugal effects are important in Saturn's magnetosphere and these exert a southward force which pushes plasma toward the rotational equator. This does not invalidate our analysis because if the current sheet did lie in the rotational equator, one would find the opposite result that the spacecraft was northward, not southward of the dipole equator. Furthermore, the $0.04R_S$ offset between the rotational and dipole magnetic equators is small and so our results are consistent with the current sheet being located northward of both the rotational and dipole magnetic equators.

[15] To establish the dependence over all local times in a statistical sense, Figure 6 shows the sign of the radial field as a function of radial (cylindrical) distance from the spin axis and vertical distance above and below the dipole magnetic equator for 25 orbits of Cassini, covering 22 months of magnetometer observations inside the magnetosphere. The measurements typically come from the fluxgate instrument, but data from the vector helium instrument is used to fill data gaps when necessary. The data shown on Figure 6 are 5 min averages produced by a boxcar algorithm. Data outside the last inbound and first outbound magnetopause crossings are excluded on each orbit. The transition between gray ($B_r \geq 0$) and black ($B_r < 0$) orbit segments should occur at $Z_{DIP} = 0$ where the dipole magnetic equator is located. This is not observed beyond $14R_S$ in the local time sectors covered by Figure 6, over a range of 0100–1300 SLT.

[16] One must also take into account the geometric thickness of the current sheet which places additional constraints on the distortion of the current sheet. From the absence of field fluctuations in Figure 4 and the magnitude of B_r compared to B_z, one concludes that Cassini is in the lobe-type regions bounding a thin current sheet. Simple axisymmetric models of such current sheets in Saturn's magnetosphere [e.g., *Giampieri and Dougherty*, 2004; *Dougherty et al.*, 2005, G. Giampieri, private communication, 2005] suggest a current sheet half-thickness of $2R_S$. Hence if Cassini is near the rotational equator and observing lobe-type fields one is forced to conclude that the spacecraft is around $2R_S$, or more, from the center of the current sheet and the magnetic equator.

2.2. Interpretation

[17] We interpret the current sheet distortion or "hinging" in terms of solar wind forcing on the magnetosphere. The normal stress exerted on the magnetosphere when the dipole is perpendicular to the equator acts to compress the dayside but does not shift the location of the magnetic equator. When the dipole magnetic equator is tilted with respect to the solar wind the pressure the most important effect, to first order, is still to compress the dayside. However, the normal stress acting perpendicular to the current sheet displaces the current sheet out of the equator. Hence we argue that the magnetospheric current sheet is displaced northward (southward) over all local times for negative (positive) magnetospheric tilt angles. This should also be true for the as yet unobserved dusk flank. This does not necessarily imply that the displacement will be symmetric in local time.

[18] The most obvious source of magnetospheric symmetry breaking is the solar wind forcing on a tilted dipole however there are other sources of symmetry breaking, such as the presence of magnetic anomalies, mass loading effects, and dynamic features such as reconnection and particle injection. Dynamic features introduce transient asymmetries on small spatial scales and so would not reproduce the large-scale distortion that is observed. A magnetic anomaly inside the planet would produce an asymmetry that rotated with the planet and thus would produce a longitudinal asymmetry, not a global distortion. We have accounted for the north-south asymmetry in the magnetic field due to the quadrupole and octupole moments of the internal field.

[19] Mass loading mainly introduces asymmetries localized near moons and other neutral sources. In principle, a large-scale neutral source (such as Saturn's OH neutral cloud) with a pronounced persistent asymmetry about Saturn's equator could produce the observed field distortion. *Esposito et al.* [2005] used data from Cassini's approach to Saturn to study the distribution of Saturn's OH neutral cloud. An examination of the figures in the work of *Esposito et al.* [2005] shows that the neutral cloud does not have a pronounced north-south asymmetry, thus arguing against a mass loading interpretation for the observed distortion.

[20] In support of our interpretation we observe that the current sheet is displaced from its nominal location when the magnetospheric magnetic pressure is comparable to or less than typical dynamic pressures of the solar wind (Figures 3e, 4e, and 5e).

[21] It is well-known that the mean location of the Jovian magnetodisc can change abruptly and remain in the same configuration for a number of days [e.g., *Goertz*, 1981; *Vasyliunas et al.*, 1997]. Because the warping is driven by the solar wind, a change in the intensity of the solar wind momentum flux should result in the current sheet becoming warped closer to, or farther from, the planet. At Saturn's orbit the solar wind dynamic pressure can vary by approximately an order of magnitude (N. Achilleos et al., Large-scale dynamics of Saturn's magnetopause: Observations by Cassini, manuscript in preparation for *Journal of Geophysical Research*, 2008) according to a pattern of compression and rarefaction regions in the solar wind [*Jackman et al.*, 2004]. These compression regions are associated with intervals of elevated dynamic pressure and can persist for several days.

[22] Evidence for such persistent changes in current sheet location have been identified. Figure 7 shows magnetometer data and a plasma electron time-energy spectrogram (from the CAPS ELS instrument [*Young et al.*, 2004]) from 11 to 14 May 2006 during Cassini's Rev 24. Periodic perturbations in the magnetic field and thermal electrons are visible approximately every 11 h and allow us to track changes in the current sheet location. We will consider these periodic features in the discussion. In the middle of the plot the magnetic field becomes disturbed for approximately two rotations of Saturn and an examination of the electron spectrogram shows that Cassini was located much closer to the plasma sheet during the more disturbed interval. We suggest that this disruption to the regular pattern of perturbations is driven by a change in the upstream solar wind conditions producing a change in the mean location of the current sheet.

3. Modeling the Current Sheet Shape

[23] Saturn's magnetospheric current sheet dominates the external magnetic field and has an important role in the global configuration of the magnetosphere. The availability of empirical models describing the location of the current sheet is crucial in interpreting science data, studying periodicities in fields and particles, planning future missions, and developing empirical models of magnetospheric fields and particles. In this section we will present a first-order model for the mean location of Saturn's magnetospheric current sheet.

[24] Model current sheet surfaces have been constructed for Jupiter's magnetodisc and Earth's magnetotail current sheets using a variety of functional forms [e.g., *Khurana and Schwarzl*, 2005; *Tsyganenko and Fairfield*, 2004, and references therein]. The functional forms used to model the current sheet surface are chosen so they can flexibly model the surface as a function of local time, distance, magnetic dipole axis orientation, and upstream solar wind conditions.

[25] To model the shape of Saturn's bowl-shaped current sheet, we work in cylindrical coordinates (r, ϕ, z), where r and ϕ are in the rotational equator and z is the distance from the rotational equator. We adapted existing functional forms developed for Jupiter and eliminated the periodic factors required by a significant dipole tilt. The selected functional form is essentially a differentiable approximation to a discontinuous piecewise surface: $z_{CS} = 0$ for $r \langle R_H$ and $z_{CS} = z_0 + z_1 r$ for $r\rangle R_H$. Equation (1) describes our model current sheet surface and represents the distance from the rotational equator to the current sheet, measured along a direction parallel to Saturn's spin axis.

$$z_{CS} = \left[r - R_H \tanh\left(\frac{r}{R_H}\right)\right] \tan\theta_{SUN} \tag{1}$$

The model is a function of cylindrical radial distance r (in the rotational equator) and is parameterized by the hinging distance, R_H, and the solar wind latitude, θ_{SUN}. These parameters are illustrated schematically in Figure 8. The solar wind latitude is the angle between Saturn's rotational equator and the solar wind flow and is defined as positive when the dipole moment points away from the Sun. Figure 8 is drawn for positive solar wind latitudes.

[26] The hinging distance is the characteristic distance from the planet where the current sheet no longer lies in the magnetic dipole equator and does not possess planar geometry, although in this model the warping is gradual and the hinging distance is a characteristic distance at which this warping starts to occur. From modeling of the terrestrial [e.g., *Tsyganenko and Fairfield*, 2004] and Jovian magnetospheres [e.g., *Khurana and Schwarzl*, 2005] this hinging distance is typically the average distance from the planet to the subsolar magnetopause. The subsolar distance to Saturn's dayside magnetopause has been found to lie between approximately 17 and $30R_S$ (Achilleos et al., manuscript in preparation, 2008) and hence by analogy we expect the hinging distance to be approximately $25R_S$.

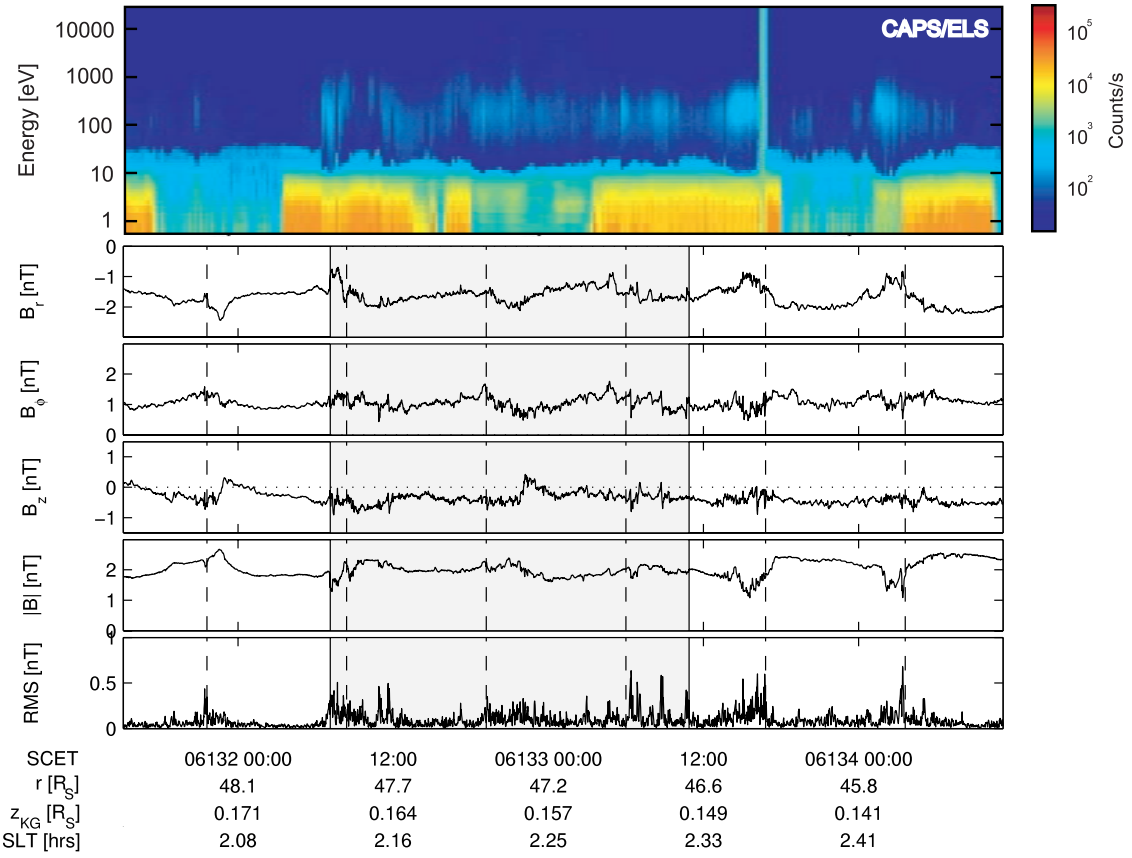

Figure 7. Magnetometer data and an electron spectrogram from the CAPS/ELS instrument. (top) The 640 s averages of the count rates of electrons measured between 0.5 eV and 28 keV. The intense and variable electron fluxes in the energy channels below approximately 20 eV are spacecraft photoelectrons. (middle) The three components of the magnetic field in cylindrical polar coordinates and the field magnitude. (bottom) The root-mean-square fluctuation in the field, calculated from the sum of the square deviations of each field component from a 15 min mean: $RMS_i = \sum_{j=0,1,2}(B_{ij} - \langle B_j \rangle_i)^2$. Vertical lines are drawn every 10.8 h to guide the eye to the periodic features in the data, occurring approximately every 11 h. The marked region highlights a clear disruption to the clean periodic signal.

[27] It is important to note that the selected functional form (1) is symmetric in local time by construction. It is quite natural to assume that since the magnetosphere is asymmetric in local time, the distortion of the current sheet will also be asymmetric. It would be quite straightforward to make the hinging distance some function of local time although the hinging distance will also be a function of solar wind dynamic pressure. The identification of such a local time and pressure dependence is beyond the scope of this paper and will be reported separately.

[28] Modeling studies of the terrestrial and Jovian current sheets use large databases of current sheet crossings to obtain the best-fit values of each model parameter. Current sheet crossings have been observed by Cassini in a limited radial and local time range because of a combination of the spacecraft trajectory and the lack of diurnal motions of Saturn's current sheet. Although diurnal motions have been observed in Saturn's magnetotail, these are not yet sufficiently characterized or spatially distributed and preclude such an optimization to find the best-fit model parameters.

[29] To identify the most appropriate hinging distance, the efficiency (percentage of correct identifications) of the model in predicting the correct sign of B_r was assessed for different values of the hinging distance. This analysis would produce a peak in the efficiency for the most appropriate value of R_H. Figure 9 shows the results of this optimization and plots the efficiency of predicting the correct sign of B_r as a function of R_H. The peak prediction efficiency occurs at $R_H = 29R_S$ and is in good agreement with the analogy presented above. This analysis was carried out using 1 min resolution magnetometer data and includes data from SOI to 9 February 2007. To avoid introducing bias, the data was resampled so that there equal numbers of samples of positive and negative B_r.

[30] Figure 10 presents a comparison of the radial component of the magnetic field and the location of the model current sheet surface. The radial component of the field should reverse in sense about the current sheet, i.e., $B_r = 0$ along the current sheet surface. Although Cassini does not cover higher latitudes at larger radial distances in the dusk sector, the agreement in Figure 10 is excellent in each local time sector with reasonable coverage.

[31] The schematic presented in Figure 8 shows the shape of the bowl-shaped current sheet in two inertial coordinate

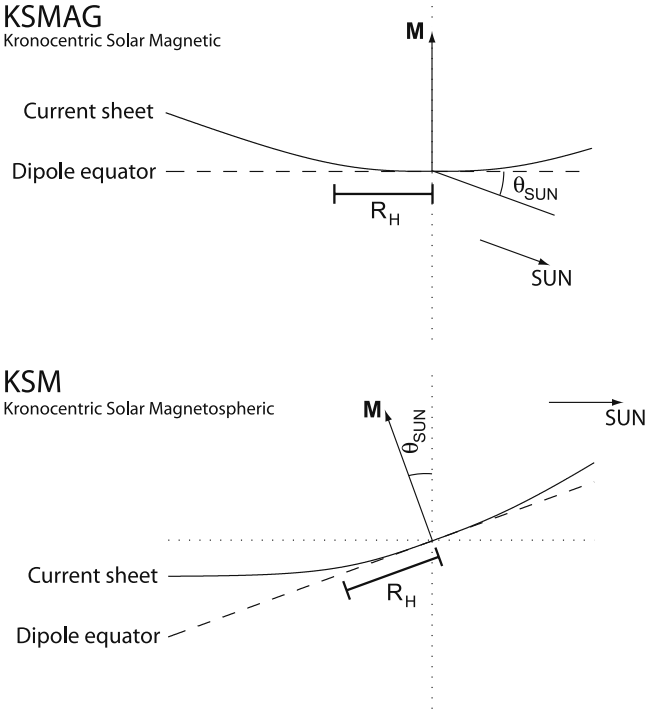

Figure 8. Schematic illustrating the bowl-shaped model as represented in two different coordinate systems, KSMAG and KSM. The direction of the Sun and the magnetic dipole axis **M** are illustrated in both systems. The figure also illustrates the physical meaning of the two parameters in equation (1); the hinging distance, R_H, and the latitude of the Sun, θ_{SUN}.

frames, Kronocentric Solar Magnetic (KSMAG) and Kronocentric Solar Magnetospheric (KSM) (defined in Appendix B). KSMAG is essentially a despun version of Kronographic (KG) coordinates where the X axis is oriented toward the Sun. Hence assuming azimuthal symmetry our model surface (1) gives the distance of the current sheet, from the rotational equator, measured along the Z axis in both the KG and KSMAG frames, and the radial distance r is simply the distance measured in the X-Y planes of both frames.

[32] It is straightforward to transform the current sheet surface from KSMAG into more familiar KSM coordinates. One may simply rotate the surface about the Y axis by the solar wind latitude (see Appendices A and B). Hence the current sheet surface in the noon-midnight meridian of KSM can be written as:

$$\begin{aligned} x_{KSM,CS} &= x_{KSMAG,CS}\cos\theta_{SUN} - \left[r - R_H\tanh\left(\frac{r}{R_H}\right)\right] \\ &\quad\cdot\tan\theta_{SUN}\sin\theta_{SUN} \\ z_{KSM,CS} &= x_{KSMAG,CS}\sin\theta_{SUN} + \left[r - R_H\tanh\left(\frac{r}{R_H}\right)\right] \\ &\quad\cdot\tan\theta_{SUN}\cos\theta_{SUN} \end{aligned} \tag{2}$$

It is straightforward to calculate the distance from a spacecraft to the current sheet, measured along the local normal to the sheet. The quantity $z_{CS} - z_{SC}$ is the distance between the current sheet and the spacecraft measured along Saturn's spin axis, and $(z_{CS} - z_{SC})\cos\theta_n$ is the same quantity measured along the local normal [*Khurana and Kivelson*, 1989]. Here θ_n is the angle between Saturn's spin axis and the local normal to the current sheet and can be calculated from $\cos^{-1}(\frac{\mathbf{n_{CS}}\hat{\mathbf{Z}}_{\mathbf{KG}}}{|\mathbf{n_{CS}}|})$ where $\mathbf{n_{CS}} = (-\tan\theta_{SUN}\tanh^2(r/R_H), 0, 1)$ in cylindrical coordinates. Clearly, close to Saturn the difference between these two quantities will be small and up to $\sim 25R_S$ the error in assuming $\cos\theta_n = 1$ is less than 20% but increases rapidly beyond $30R_S$.

[33] We will now present an application of this shape model to correct simple axisymmetric models of Saturn's current sheet.

4. Application to Modeling the Current Sheet Magnetic Field

[34] Saturn's ring current has traditionally been modeled using the *Connerney et al.* [1981] current sheet model (hereinafter referred to as the CAN81 model) originally developed to represent the Jovian magnetodisc. This model and its subsequent analytic approximations [e.g., *Giampieri and Dougherty*, 2004] have been applied to produce global magnetospheric models [e.g., *Maurice and Engle*, 1995; *Dougherty et al.*, 2005], examine the response of the ring current to changes in solar wind dynamic pressure [*Bunce et al.*, 2007], and to examine the force balance associated with the ring current [*McNutt*, 1984], amongst other applications. Despite the fact that the CAN81 model does not appear to provide a reasonable representation of the local ring current density and magnetic stress [e.g., *Mauk et al.*, 1985; *Vasyliunas*, 1983], it does provide a reasonable representation for the magnetic field of the ring current; see for example comparisons in the work of *Dougherty et al.* [2005] and *Bunce et al.* [2007].

[35] The CAN81 model is a washer-shaped azimuthally symmetric current sheet with a rectangular cross section in

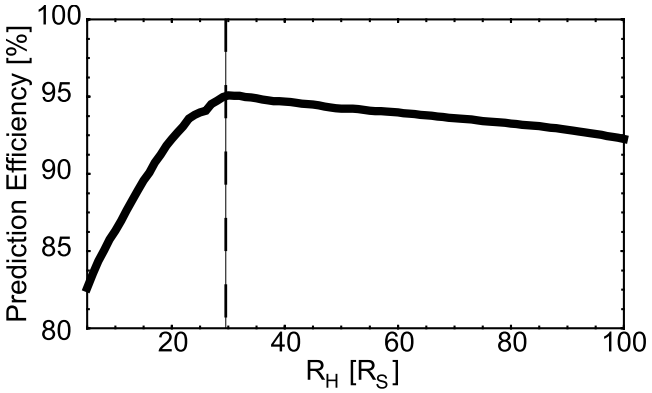

Figure 9. The efficiency of correctly predicting the sign of B_r and hence of correctly modeling the location of Cassini with respect to the current sheet as a function of the hinging distance, R_H. This provides a simple method to identify the most optimal hinging distance, without fitting a global magnetospheric magnetic field model (incorporating the bowl shape) to a large database of magnetic field measurements. The optimal hinging distance found by this technique is around $29R_S$.

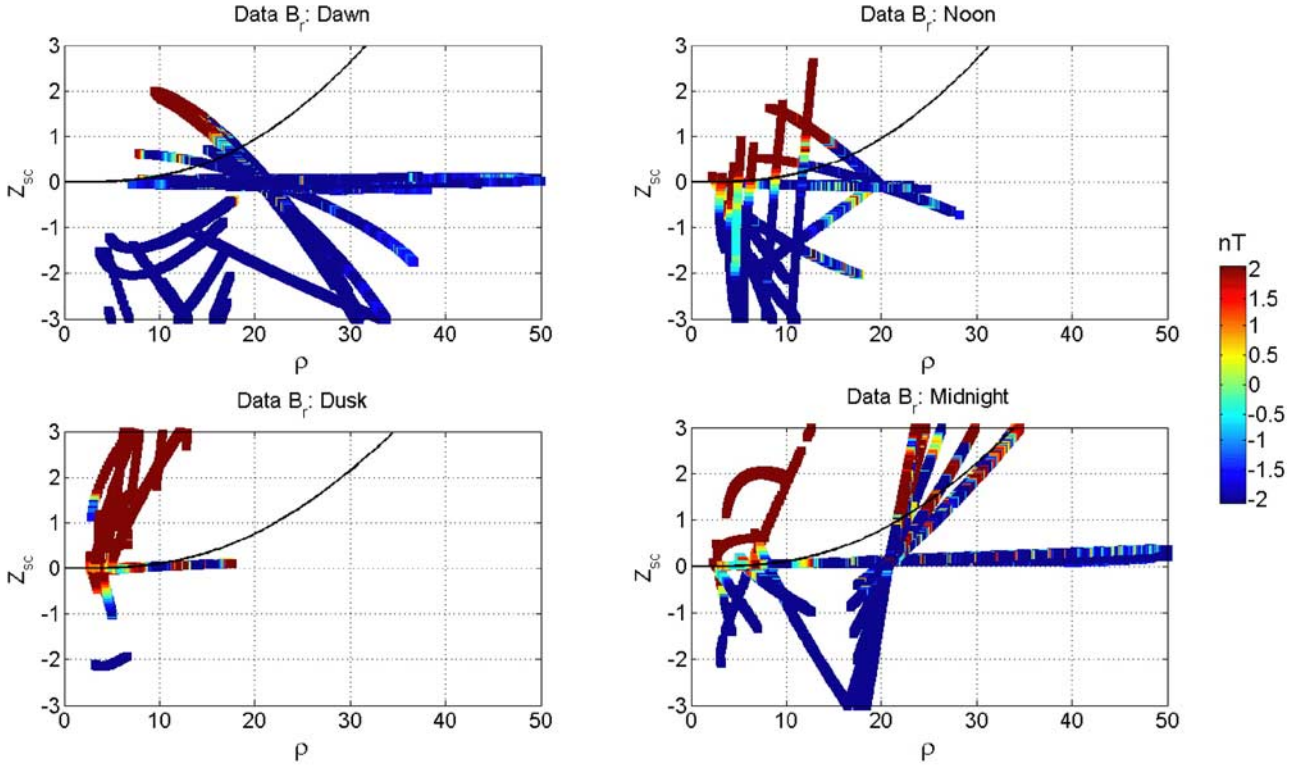

Figure 10. The value of the radial magnetic field component plotted along the spacecraft trajectory in KG coordinates, with cylindrical radial distance along abscissa and the vertical distance above the rotational equator on the ordinate axis. The colored squares indicate the value of B_r in nT and were produced from 1 min resolution magnetometer data from SOI to 9 February 2007 but were decimated by a factor of 10 for plotting. The model current sheet surface is indicated by the solid line. Neglecting dynamical features the positive and negative radial fields are evenly distributed about the model current sheet location.

the (r, z) plane. The model is parameterized by four quantities, the inner and outer edges of the current sheet, a and b, the half-thickness of the current sheet, D, and a scaling parameter, I_0, which describes the strength of the current sheet. This scaling parameter is often given as the product $\mu_0 I_0$ in units of teslas. The volume current density in the sheet is given by $j_\phi = I_0/r$. In all previous studies at Saturn the center of the current sheet was placed in the rotational equator, although at Jupiter, *Connerney et al.* [1981] found improved fits could be obtained by placing the current sheet in the centrifugal equator (lying between the rotational and dipole equators) rather than in the dipole magnetic equator.

[36] Figure 11 compares the field from the CAN81 model (placed in the rotational equator) with the magnetometer data presented in Figure 4. To produce Figure 11, a model for Saturn's internal magnetic field [*Dougherty et al.*, 2005] was subtracted from the observed magnetic field vectors to produce the residual field $\Delta\mathbf{B}$. This field essentially represents the field due to the magnetospheric current systems. These data are plotted in cylindrical polar coordinates and we suppress the azimuthal component because of the symmetry of the CAN81 model.

[37] The red curves show the output from the CAN81 model with inner and outer edges at $a = 6.32R_S$ and $b = 31.7R_S$, respectively, a half-thickness of $D = 2.0R_S$, and strength of $\mu_0 I_0 = 50nT$. From an inspection of Figure 11 it is clear that the model does not provide a good fit to the residual magnetic field vectors. Since Cassini is within a few thousand kilometers of the rotational equator, no reasonable modification of these parameters can substantially improve the fit, within the context of an undeformed current sheet. In physical terms the field must reverse in sense about the center of the current sheet and hence $B_r(z = 0) = 0$. From the CAN81 model one can see that $B_r(z = 0) = 0$ since at $z = 0$ the Legendre polynomials cancel (equation (4) of *Giampieri and Dougherty* [2004]).

[38] Figure 11 clearly demonstrates the need to include the warping of the current sheet in any empirical model. In general simply deforming a magnetic field leads to a violation of $\nabla \cdot \mathbf{B} = 0$. A particularly elegant method of modeling warped and deformed configurations using Euler potentials, thus preserving $\nabla \cdot \mathbf{B} = 0$, was presented by *Tsyganenko* [1998] and extended an earlier Cartesian development by *Stern* [1987]. We will briefly outline this method and its derivation and then apply this in cylindrical coordinates to deform the CAN81 model using the geometry model presented in equation (1).

[39] Let us write the undeformed (CAN81) field $\mathbf{B}$ as a function of a set of orthonormal coordinates (f, g, h) and

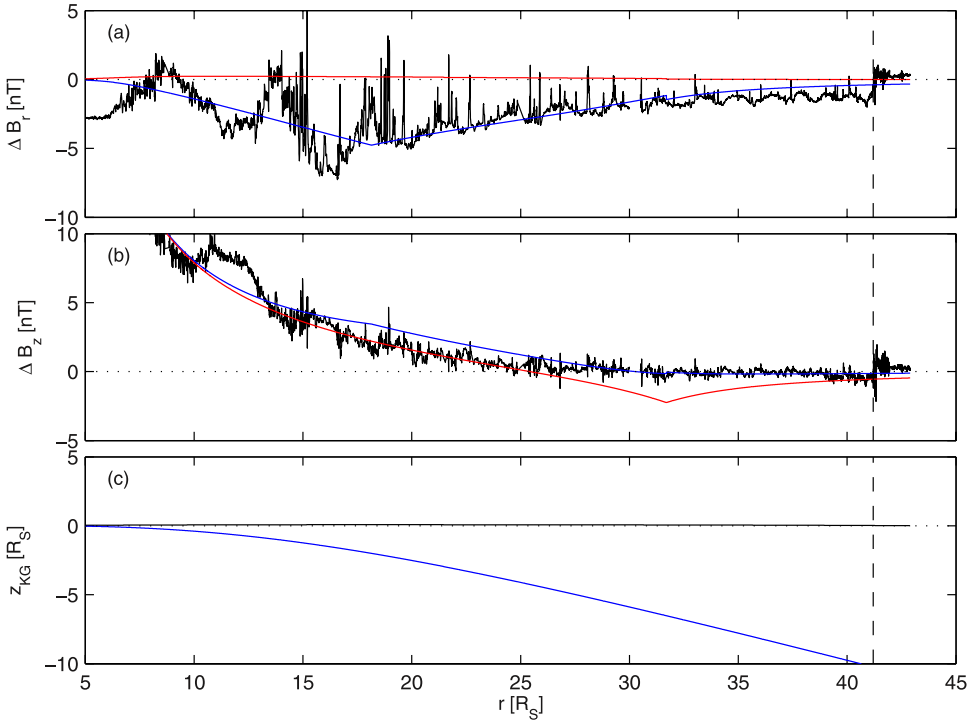

Figure 11. Modeling results for Cassini's rev 3 outbound pass on the dawn flank from 17 to 21 February 2005. (a) and (b) The radial and axial components (respectively) of the residual magnetic field (in black) obtained by subtracting a model internal field from the observed magnetic field. The azimuthal component is not plotted due to the axisymmetry of the CAN81 model. (c) The distance of Cassini from the rotational equator. The red curves in Figures 11a and 11b show the model curves from the CAN81 model which has been placed in Saturn's rotational equator. The blue curves in Figures 11a and 11b are the result of warping the CAN81 model using the bowl-shape model (1). The blue curve in Figure 11c shows the mapped spacecraft location according to this model illustrating that Cassini is underneath the current sheet.

suppose that we can express this field using a pair of Euler potentials, α and β.

$$\mathbf{B}(f,g,h) = \nabla\alpha(f,g,h) \times \nabla\beta(f,g,h) \tag{3}$$

The deformed field representing the bowl-shaped CAN81 field is denoted $\mathbf{B}'$ and is also written in the undeformed orthonormal basis ($\mathbf{e_f}$, $\mathbf{e_g}$, $\mathbf{e_h}$). From the definition of the Euler potentials in terms of the unit vectors and scale factors $\{H_f, H_g, H_h\}$ for the coordinates (f, g, h) we can write the undeformed field as:

$$\begin{aligned} B_f &= \frac{1}{H_g H_h}\left(\frac{\partial\alpha}{\partial g}\frac{\partial\beta}{\partial h} - \frac{\partial\beta}{\partial g}\frac{\partial\alpha}{\partial h}\right) \\ B_g &= \frac{1}{H_f H_h}\left(\frac{\partial\alpha}{\partial h}\frac{\partial\beta}{\partial f} - \frac{\partial\beta}{\partial h}\frac{\partial\alpha}{\partial f}\right) \\ B_h &= \frac{1}{H_f H_g}\left(\frac{\partial\alpha}{\partial f}\frac{\partial\beta}{\partial g} - \frac{\partial\beta}{\partial f}\frac{\partial\alpha}{\partial g}\right) \end{aligned} \tag{4}$$

The deformation consists of mapping each point in the undeformed field to a set of new (mapped or deformed) points ($\zeta(f, g, h)$, $\eta(f, g, h)$, $\xi(f, g, h)$). At these mapped coordinates the field $\mathbf{B}^*$ is calculated in the new orthonormal basis ($\mathbf{e}_\zeta$, $\mathbf{e}_\eta$, $\mathbf{e}_\xi$). The partial derivatives of (ζ, η, ξ) with respect to (f, g, h) are used to express the deformed field as a function of the undeformed orthonormal basis [see, e.g., *Tsyganenko*, 1998, equations (4)–(6)]. In practice this consists of calculating the coordinates (ζ, η, ξ), evaluating the field $\mathbf{B}^*$ at these coordinates, and finally applying the transformation from $\mathbf{B}^*$ to $\mathbf{B}'$.

[40] To apply this to the CAN81 and the bowl-shaped models, we construct the following mapping in cylindrical polar coordinates:

$$\begin{aligned} r &\rightarrow r \\ \phi &\rightarrow \phi \\ z &\rightarrow z + [r - R_H \tanh(r/R_H)] \tan\theta_{SUN} \end{aligned} \tag{5}$$

It is straightforward to write down the partial derivatives of this mapping and the resulting transformation from the deformed basis to the undeformed basis can be written (corresponding to *Tsyganenko* [1998, equations (5)–(6)] and example equation (13)).

$$\begin{aligned} B'_r &= B^*_r \\ B'_\phi &= B^*_\phi \\ B'_z &= -B^*_r \tan\theta_{SUN} \tanh^2(r/R_H) + B^*_z \end{aligned} \tag{6}$$

The results of applying the above deformation to the CAN81 model are plotted in blue in Figure 11 showing the

resulting model magnetic field and the mapped spacecraft location with respect to the center of the current sheet. This clearly shows that the deformed model is a substantial improvement. The parameters used for both the CAN81 model and the hinging distance ($R_H = 16R_S$) were obtained by nonlinear least squares using an interior-reflective Newton method. The same CAN81 parameters were also used to plot the undeformed red curve, but as was mentioned, no modification of these parameters can substantially improve the fit.

[41] The value of R_H obtained by the nonlinear optimization ($16R_S$) is substantially different to that obtained by the prediction efficiency analysis ($29R_S$). How can we reconcile these values? First, we should point out that the prediction efficiency was carried out on a global data set and not one from a single pass at a particular local time. Second, the hinging distance is likely to be a function of time (reflecting the upstream solar wind conditions) and also a function of local time (since it is driven by the solar wind). Hence one might not expect the two values of R_H to be equal. Third, simultaneously fitting both the hinging distance and the parameters of the CAN81 model in a nonlinear optimization introduces uncertainties due to the limitations of the CAN81 model. For example, if the strict $1/r$ dependence of the current density does not match reality, the nonlinear optimization will find the best set of parameters which match the data, thus not accurately resolving the hinging distance. A new global magnetospheric magnetic field model is currently being constructed [*Khurana et al.*, 2006b] which includes a new accurate current sheet model and which includes the bowl-shaped model. It will be possible to obtain best-fit hinging distances using this model and performing a global fit to the magnetometer data.

5. Discussion

[42] In this paper we have demonstrated that Saturn's magnetic equator, and associated magnetospheric current sheet and plasma sheet, is displaced northward of the rotational and dipole magnetic equators. Because the displacement is observed at all observed local times, we infer that, to first order, the current sheet adopts the shape of a bowl or basin. This is illustrated schematically in Figure 12. We have argued that Saturn's large obliquity and the interaction of a significant azimuthal current sheet with the solar wind causes the displacement of the magnetic equator. This contrasts with the situation at Jupiter where the current sheet becomes parallel to the solar wind flow direction both in the tail and the dayside. The distortion of the terrestrial dayside requires more detailed theoretical and numerical analysis before definitive conclusions can be drawn in a comparison between Saturn and the Earth.

[43] In our solar wind interpretation for the distortion of the current sheet, we note an interesting similarity with the distortion of Neptune's magnetosphere at certain points in its sidereal rotation, when its internal magnetic field dipole moment points into the solar wind. Such a situation is also realized in numerical MHD simulations of the Earth's paleomagnetosphere [e.g., *Zieger et al.*, 2004]. Consider a situation of very low solar wind pressure or where the solar wind has essentially disappeared. When Neptune's dipole moment is aligned with the planet-Sun line, the ring current/current sheet streamlines will lie in a plane perpendicular to the planet-Sun line. As the solar wind dynamic pressure increases the solar wind forcing on the magnetosphere will distort these streamlines so that the current sheet bends tailward forming a truncated cone with its apex towards the subsolar point.

[44] Although Saturn's dipole is not parallel to the solar wind flow, the magnetospheric tilt is relatively large. One might imagine increasing Saturn's obliquity in Figure 12 such that the dayside current sheet undergoes a more extreme distortion and approaches the neptunian configuration. Conversely, as Saturn approaches equinox the tilt between the dipole and the solar wind will drop and one might expect the sheet to eventually approach such a shallow angle that it no longer undergoes a displacement northward during Northern Hemisphere winter but is displaced southward or remains in the dipole magnetic equator.

[45] The existing structural models for the Jovian current sheet [e.g., *Khurana and Schwarzl*, 2005] do not include a solar wind displacement northward (southward) during Northern Hemisphere winter (summer) on the dayside. It is quite likely that the magnetohydrodynamic stresses responsible for forming the Jovian magnetodisc current sheet and hinging it toward the rotational equator may nullify the effect of solar wind forcing on the dayside. Furthermore, the Jovian magnetosphere is highly compressible and the noon magnetodisc is very complex and poorly ordered [e.g., *Smith et al.*, 1974]. Hence this seasonal effect may not occur or may be very difficult to detect at Jupiter. Even during northern winter, where the spin axis is tilted by 3.1° away from the sun, the actual magnetospheric tilt will vary between 12.6° and −6.5° over a spin period. So perhaps Jupiter's magnetodisc never attains a sufficiently large tilt to be distorted in a similar manner to that reported in this paper. To establish any such seasonal dayside dependence at Jupiter would require the detailed study of the current sheet, in particular System III longitude ranges corresponding to maximum magnetospheric tilt.

[46] The model presented in section 3 is a static model describing the solar wind bending of Saturn's magnetospheric current sheet. Clear observations of periodic motions of the current and plasma sheet have been detected in the magnetotail [*Carbary et al.*, 2007; *Khurana et al.*, 2006a; *Arridge et al.*, 2007] and these must be taken into account in any complete description of the geometry of Saturn's current sheet. The origin and modeling of these periodic motions is beyond the scope of this paper; however, we note that it is relatively straightforward to generalize equation (1) to include such a time-dependent geometry. This modeling will be the subject of a future publication.

[47] The implications for these results on studies of the kronian system with Cassini and future missions are significant. Plasma observations assuming a symmetric magnetosphere with the plasma sheet in the rotational equator will fail to obtain significant particle fluxes because the plasma sheet has warped with the current sheet. The construction of accurate structural models of the current sheet, ideally including time dependence, are critical to improve the science return for future Cassini observations and future mission designs.

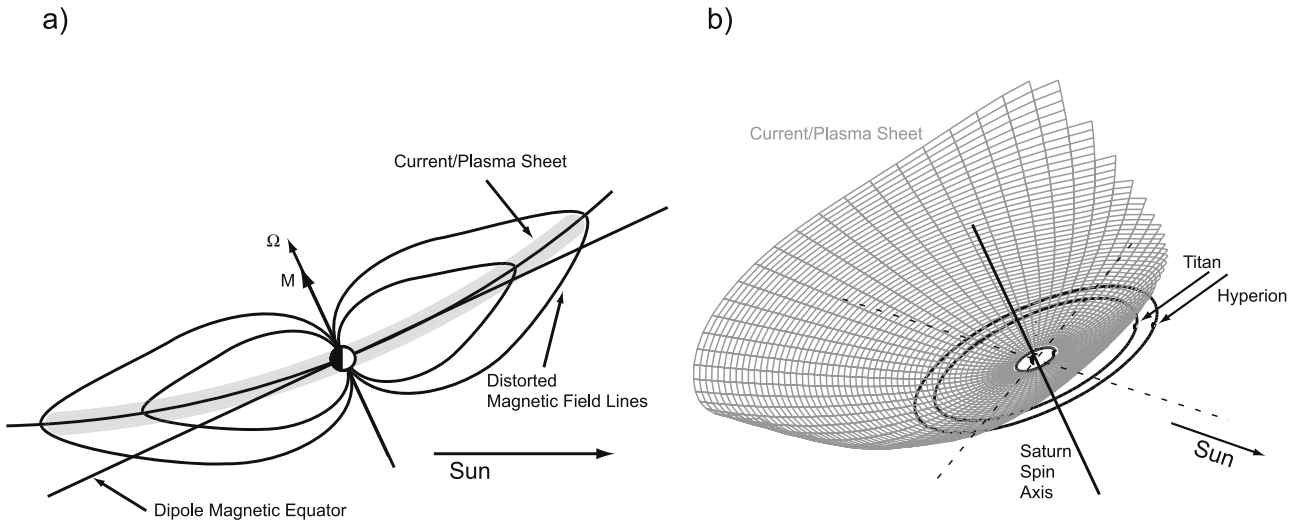

Figure 12. Schematics illustrating the distortion of Saturn's magnetosphere. (left) The distorted plasma/current sheet and magnetic field lines in the noon-midnight meridian. (right) A three-dimensional view of this distortion and the resulting bowl-shaped current sheet. The orbits of Titan and Hyperion are included showing that they are underneath the sheet. In reality the sheet has a finite thickness which varies with radial distance and local time, so even though Titan is underneath the center plane of the sheet, it is usually (near noon) immersed in the plasma sheet.

[48] We also note that the presence of a distorted current sheet has serious implications for the interaction of the magnetosphere with Titan and other more distant moons such as Hyperion. Traditionally, models of the Titan interaction assume that Titan lies in the magnetic equator. Our results clearly show that this is not the case. This implies that sometimes Titan's magnetospheric interaction will be in a lobe-type field with a low beta. The shift in Titan's magnetic latitude also changes the motional electric field in Titan's reference frame. Further studies of the impact of this distortion of Saturn's magnetic equator are required to fully understand the interaction of Titan with Saturn's magnetosphere.

Appendix A: Calculating the Latitude of the Sun

[49] The latitude of the Sun, θ_{SUN}, used in the model can be calculated in a straightforward manner using the SPICE software package and appropriate SPICE kernels. The latitude can also be found in a straightforward manner using the following expression where t_{YR} is fractional years obtained by dividing the day of year by the number of days per year.

$$\theta_{SUN} = -1.371^\circ - 25.69^\circ \cos(2.816 + 0.213499 t_{YR}) + 1.389^\circ \cos(5.4786 + 0.426998 t_{YR}) \quad \text{(A1)}$$

This was obtained by fitting the expression to a table of latitudes from 1975 to 2009 inclusive (produced from SPICE) using Marquardt's method [e.g., *Press et al.*, 1992] for nonlinear least squares. The root-mean-square error of this fit is 0.06° with a maximum error of 0.09°. For example, at Cassini Saturn Orbit Insertion (t_{FYEAR} = 2004.5) the calculated latitude using (A1) is 23.67° and the value calculated using SPICE is 23.7355°.

Appendix B: Coordinate Systems

[50] Kronocentric Solar Magnetic (KSMAG) and Kronocentric Solar Magnetospheric (KSM) are the two coordinate frames used to describe the model current sheet surface in section 3. Here we will present the definition of these two coordinate frames and describe the transformations required to move between these two frames.

[51] KSMAG is essentially a despun dipole coordinate frame and can be obtained from kronographic (KG) coordinates by despinning the KG coordinates (making the frame inertial) and then rotating around $\hat{\mathbf{e}}_\mathbf{z}$ from Saturn's vernal equinox to orient $\hat{\mathbf{e}}_\mathbf{x}$ sunward. The three unit vectors in KSMAG are defined by $\hat{\mathbf{e}}_\mathbf{z}$ pointing along the magnetic dipole axis ($\hat{\mathbf{M}}$), $\hat{\mathbf{e}}_\mathbf{z} \times \mathbf{e}_{\hat{\mathbf{SUN}}} = \hat{\mathbf{e}}_\mathbf{y}$, and $\hat{\mathbf{e}}_\mathbf{x}$ completing the right-hand orthogonal set and lying in the plane formed by the magnetic dipole axis and the sun direction unit vector.

[52] KSM is the kronian analogue of GSM; $\hat{\mathbf{e}}_\mathbf{x}$ points to the Sun, $\hat{\mathbf{M}} \times \hat{\mathbf{e}}_\mathbf{x} = \hat{\mathbf{e}}_\mathbf{y}$, and $\hat{\mathbf{e}}_\mathbf{z}$ completes the right-hand set and lies in the plane formed by the magnetic dipole axis and the sun direction unit vector.

[53] These two frames share a common Y axis and thus clearly, KSM can be obtained from KSMAG by a rotation around $\hat{\mathbf{e}}_\mathbf{y}$ by the solar wind latitude:

$$\begin{aligned} x_{KSM} &= x_{KSMAG} \cos\theta_{SUN} - z_{KSMAG} \sin\theta_{SUN} \\ y_{KSM} &= y_{KSMAG} \\ z_{KSM} &= x_{KSMAG} \sin\theta_{SUN} + z_{KSMAG} \cos\theta_{SUN} \end{aligned} \quad \text{(B1)}$$

[54] **Acknowledgments.** CSA would like to acknowledge useful discussions with N. André, C. Bertucci, S.W.H. Cowley, I. Dandouras, G.H. Jones, N. Krupp, and D.G. Mitchell, and both referees for their

extensive and detailed comments. The authors acknowledge S. Kellock, P. Slootweg, and T. Sears at Imperial College for MAG data processing and L.K. Gilbert and G.R. Lewis for CAPS/ELS data processing at MSSL/UCL. CSA was supported in this work by a PPARC quota studentship to Imperial College and by the STFC rolling grant to MSSL/UCL. CTR and KKK were supported by NASA. AJC was supported by the STFC rolling grant to MSSL/UCL.

[55] Wolfgang Baumjohann thanks the reviewers for their assistance in evaluating this paper.

References

Arridge, C. S., N. Achilleos, M. K. Dougherty, K. K. Khurana, and C. T. Russell (2006), Modeling the size and shape of Saturn's magnetopause with variable dynamic pressure, *J. Geophys. Res.*, *111*, A11227, doi:10.1029/2005JA011574.

Arridge, C. S., et al. (2007), Plasma electrons in Saturn's magnetotail, paper presented at the Magnetospheres of the Outer Planets meeting, Southwest Res. Inst., San Antonio, Tex.

Arridge, C. S., C. T. Russell, K. K. Khurana, N. Achilleos, S. W. H. Cowley, M. Dougherty, D. J. Southwood, and E. J. Bunce (2008), Saturn's magnetodisc current sheet, *J. Geophys. Res.*, *113*, A04214, doi:10.1029/2007JA012540.

Bagenal, F. (1992), Giant planet magnetospheres, *Annu. Rev. Earth Planet. Sci.*, *20*, 289–328.

Bunce, E. J., S. W. H. Cowley, I. I. Alexeev, C. S. Arridge, M. K. Dougherty, J. D. Nichols, and C. T. Russell (2007), Cassini observations of the variation of Saturn's ring current parameters with system size, *J. Geophys. Res.*, *112*, A10202, doi:10.1029/2007JA012275.

Carbary, J. F., D. G. Mitchell, S. M. Krimigis, D. C. Hamilton, and N. Krupp (2007), Spin-period effects in magnetospheres with no axial tilt, *Geophys. Res. Lett.*, *34*, L18107, doi:10.1029/2007GL030483.

Connerney, J. E. P., M. H. Acuña, and N. F. Ness (1981), Modeling the Jovian current sheet and inner magnetosphere, *J. Geophys. Res.*, *86*(A10), 8370–8384.

Dougherty, M. K., et al. (2004), The Cassini magnetic field investigation, *Space Sci. Rev.*, *114*, 331–383.

Dougherty, M. K., et al. (2005), Cassini magnetometer observations during Saturn orbit insertion, *Science*, *307*, 1266–1270.

Esposito, L. W., et al. (2005), Ultraviolet Imaging Spectroscopy Shows an Active Saturnian System, *Science*, *307*, 1251–1255.

Giampieri, G., and M. K. Dougherty (2004), Modelling of the ring current in Saturn's magnetosphere, *Ann. Geophys.*, *22*(1), 653–659.

Goertz, C. K. (1981), The orientation and motion of the predawn current sheet and Jupiter's magnetotail, *J. Geophys. Res.*, *86*(A10), 8429–8434.

Hill, T. W., A. J. Dessler, and F. C. Michel (1974), Configuration of the Jovian magnetosphere, *Geophys. Res. Lett.*, *1*(1), 3–6.

Jackman, C. M., N. Achilleos, E. J. Bunce, S. W. H. Cowley, M. K. Dougherty, G. H. Jones, S. E. Millan, and E. J. Smith (2004), Interplanetary magnetic field at $\approx 9AU$ during the declining phase of the solar cycle and its implications for Saturn's magnetospheric dynamics, *J. Geophys. Res.*, *109*, A11203, doi:10.1029/2004JA010614.

Khurana, K. K. (1992), A generalized hinged-magnetodisc model of Jupiter's nightside current sheet, *J. Geophys. Res.*, *97*(A5), 6269–6276.

Khurana, K. K., and M. G. Kivelson (1989), On Jovian plasma sheet structure, *J. Geophys. Res.*, *94*(A9), 11,791–11,803.

Khurana, K. K., and H. K. Schwarzl (2005), Global structure of Jupiter's magnetospheric current sheet, *J. Geophys. Res.*, *110*, A07227, doi:10.1029/2004JA010757.

Khurana, K. K., C. S. Arridge, M. K. Dougherty, and C. T. Russell (2006a), Periodic crossings of Saturn's current sheet by Cassini: Observations and modeling, *Eos. Trans. AGU*, *87*(52), Fall Meet. Suppl., Abstract SM21E-05.

Khurana, K. K., C. S. Arridge, H. Schwarzl, and M. K. Dougherty (2006b), A model of Saturn's magnetospheric field based on latest Cassini observations, *Eos Trans. AGU*, *87*(36), Jt. Assem. Suppl., Abstract P44A-01.

Kivelson, M. G., J. Warnecke, L. Bennett, S. Joy, K. K. Khurana, J. A. Linker, C. T. Russell, R. J. Walker, and C. Polanskey (1998), Ganymede's magnetosphere: Magnetometer overview, *J. Geophys. Res.*, *103*(E9), 19,963–19,972.

Mauk, B. H., S. M. Krimigis, and R. P. Lepping (1985), Particle and field stress balance within a planetary magnetosphere, *J. Geophys. Res.*, *90*(A9), 8253–8264.

Maurice, S., and I. M. Engle (1995), Idealized Saturn magnetosphere shape and field, *J. Geophys. Res.*, *100*(A9), 17,143–17,151.

McNutt, R. L. (1984), Force Balance in outer planet magnetospheres, in *Physics of Space Plasmas, Proceedings of the 1982-4 MIT Symposia*, edited by J. Belcher et al, *SPI Conf. Proc. and Reprint Ser.*, vol. 5, pp. 179–210, Scientific, Gainesville, Fla.

Press, W. H., S. A. Teukolsky, W. T. Vetterling, and B. P. Flannery (1992), *Numerical Recipes in C: The Art of Scientific Computing*, 2nd ed., Cambridge Univ. Press, New York.

Smith, E. J., L. Davis, D. E. Jones, P. J. Coleman, D. S. Colburn, P. Pyal, C. P. Sonett, and A. M. A. Frandsen (1974), The planetary magnetic field and magnetosphere of Jupiter: Pioneer 10, *J. Geophys. Res.*, *79*(25), 3501–3513.

Stern, D. P. (1987), Tail modeling in a stretched magnetosphere: 1. Methods and transformations, *J. Geophys. Res.*, *92*(A5), 4437–4448.

Tsyganenko, N. A. (1998), Modeling of twisted/warped magnetospheric configurations using the general deformation method, *J. Geophys. Res.*, *103*(A10), 23,551–23,563.

Tsyganenko, N. A., and D. H. Fairfield (2004), Global shape of the magnetotail current sheet as derived from Geotail and Polar data, *J. Geophys. Res.*, *109*, A03218, doi:10.1029/2003JA010062.

Vasyliunas, V. M. (1983), Plasma distribution and flow, in *Physics of the Jovian Magnetosphere*, edited by A. Dessler, chap. 11, pp. 395–453, Cambridge Univ. Press, New York.

Vasyliunas, V. M., L. A. Frank, K. L. Ackerson, and W. R. Paterson (1997), Geometry of the plasma sheet in the midnight-to-dawn sector of the Jovian magnetosphere: Plasma observations with the Galileo spacecraft, *Geophys. Res. Lett.*, *24*(8), 869–872.

Waldrop, L. S., T. A. Fritz, M. G. Kivelson, K. Khurana, N. Krupp, and A. Lagg (2005), Jovian plasma sheet morphology: particle and field observations by the Galileo spacecraft, *Planet. Space Sci.*, *53*, 681–692.

Young, D. T., et al. (2004), Cassini plasma spectrometer investigation, *Space Sci. Rev.*, *114*, 1–112.

Zieger, B., J. Vogt, K. H. Glassmeier, and T. I. Gombosi (2004), Magnetohydrodynamic simulation of an equatorial dipolar paleomagnetosphere, *J. Geophys. Res.*, *109*, A07205, doi:10.1029/2004JA010434.

N. Achilleos, Atmospheric Physics Laboratory, University College London, London WC1E 6BT, UK.

C. S. Arridge and A. J. Coates, Mullard Space Science Laboratory, University College London, Holmbury St. Mary, Dorking RH5 6NT, UK. (chris.arridge@physics.org)

M. K. Dougherty, Space and Atmospheric Physics Group, Blackett Laboratory, Imperial College London, London SW7 2BZ, UK.

K. K. Khurana, H. K. Leinweber, and C. T. Russell, Institute of Geophysics and Planetary Physics, University of California, Los Angeles, CA 90095-1567, USA.

D. J. Southwood, European Space Agency, F-75738 Paris CEDEX 15, France.